IEEJ Journal of Industry Applications
Vol.10 No.2 pp.214–220 DOI: 10.1541/ieejjia.20001168

Paper

Passive Rectifier for Vibration Generators based on Piezoelectric Elements with *LC* Resonance

Masataka Minami[*a)] Member, Koharu Kondo[*,**] Student Member
Shin-ichi Motegi[*] Member, Masakazu Michihira[*] Member

(Manuscript received Feb. 16, 2020, revised Dec. 4, 2020)
J-STAGE Advance published date : Dec. 25, 2020

Energy harvesting systems have recently garnered significant attention. Mechanical vibrations are used as a type of energy source in such systems. However, it is important to improve the performance of vibration generators because they provide low power in the milliwatt or microwatt level. This study investigated the improvements in the output power using passive devices. A boost-type, current-improving passive rectifier was used in this study. Additionally, an input series inductor was employed to resonate the internal capacitor of the piezoelectric elements; consequently, the output power was increased. The validity of the proposed circuit was verified both numerically and experimentally.

Keywords: energy harvesting, vibration generators, piezoelectric elements, *LC* resonance, all-passive rectifier, boost-type current-improving passive rectifier

1. Introduction

Energy harvesting systems have attracted increased attention recently [1]. Energy source is everywhere around us: wind, mechanical vibration, stress, strain, waste heat, sun light or room light, electromagnetic ray, chemical or biological sources, and so on [2]. Vibration generators based on piezoelectric elements have been highlighted as low-power sources [3].

Vibration sources are found in familiar places [4]. Platt et al. [5] made an effort to develop a piezoelectric setup in an artificial knee. Donelan et al. [6] proposed a biomechanical energy harvester, which can use knee movements to generate electrical energy. Mateu et al. [7] performed a study where they placed two piezoelectric layers, connected in parallel in a shoe to improve the output power. They investigated the configuration of the inserted beams in the shoe for power optimization. Granstrom et al. [8] proposed a novel idea to produce electrical energy using the dynamic behavior between a backpack and its wearer. Priya et al. [9] proposed a piezoelectric windmill that connected to a regular fan through a camshaft. Pobering et al. [10] demonstrated the energy harvesting possibilities from the flowing water. Oh et al. [11] demonstrated a complete tree-shaped wind driven energy harvesting system.

However, the vibration generators provide very low power around the milliwatt or microwatt level. The performance improvement of the vibration generators is required for utilization [12]. Maximum power transfer occurs when the load impedance is the complex conjugate of the source impedance. Ottman et al. [13] presented an adaptive control with a buck DC-DC converter. In addition, they investigated the proposed circuit by using a discontinuous conduction mode [14]. Kong et al. [15] proposed a resistive impedance matching for piezoelectric energy harvesting by controlling a buck DC-DC converter. Romani et al. [16] designed the circuit topology. The proposed circuit connected the diode bridge rectifier one by one to the piezoelectric energy harvester. Synchronized Switch Harvesting on Inductor (SSHI) aims to eliminate the effect of the capacitive term of piezoelectric generators (Guyomar et al. [17]; Ramadass and Chandrakasan [18], and Wu et al. [19]). The SSHI circuit composed of an inductor L and a switch S. The SSHI scheme minimizes the wasted energy to charge the internal capacitor of the piezoelectric elements positively using an LC resonant circuit. Especially, IC Lien, et al. [20] investigated the full electromechanical response and vibration phase-shift effect for the electrical behavior of a piezoelectric energy harvester embedded with a series-SSHI electronic interface. S. Lu and F. Boussaid [21] proposed a parallel-SSHI rectifier that does not require any external signals to detect the polarity change of the current produced by the piezoelectric elements. In addition, the rectifier for the piezoelectric energy harvesting was investigated. A full bride rectifier with passive diodes can be easily incorporated but the forward diode voltage drop can cause substantial power loss. Rincón-Mora and Yang [22] proposed a novel equivalent diode circuit. The circuit consists of a comparator and a FET for the lower power dissipation. Furthermore, about using active switching devices, Kwon et al. [23] suggested a rectifier-free circuit for piezoelectric energy harvesting. The circuit consists of two active switches, an inductor, and two diodes. Peters et al. [24] proposed a two-stage concept including passive stage and one active diode. We also proposed a circulating current control circuit, which consists of the active switching devices, for improvement of the output power [25][26].

When those systems use the active switching devices, they waste the driving energy for the active switching devices. In this paper, we propose an energy harvesting system for vibration generators based on piezoelectric elements without the

a) Correspondence to: Masataka Minami. E-mail: minami@kobe-kosen.ac.jp
* Kobe City College of Technology
8-3, Gakuenhigashi, Nishi-ku, Kobe 651-2194, Japan
** Nagaoka University of Technology
1603-1, Kamitomioka, Nagaoka, Niigata 940-2188, Japan

active switching devices. The rectifier consists of all-passive devices: an inductor, capacitors, and diodes. The inductor in the rectifier resonates the internal capacitor of piezoelectric elements, and the rectifier makes the impedance matching for vibration generators based on piezoelectric elements. Costanzo et al. [27] applied the additional non-dissipative component for the resonant electromagnetic vibration energy harvesters. This paper proposes the similar method for the piezoelectric element in the vibration generators. We proposed *LC* resonance to improve the output characteristics for the piezoelectric element in the vibration generators by using a resonator circuit [28]. The resonator circuit made *LC* parallel resonance. However, as the resonator circuit was a huge volume because of a huge inductor. Then, this paper omits the resonator circuit, but the proposed rectifier maintains *LC* series resonance by using an inductor included in the rectifier.

This paper is organized as follows. Section II represents the circuit configuration. The system consists of the piezoelectric elements for the vibration generators and all-passive rectifier. For circuit analysis, the piezoelectric elements for the vibration generators are expressed as an equivalent circuit for the impedance matching. Next, all-passive rectifier affects *LC* resonance with the internal capacitor of the piezoelectric elements for the impedance matching. Thus, the parameters of the rectifier are set to an appropriate value for the proposed method in section III. Section III numerically designs them. Finally, section IV numerically and experimentally addresses the proposed systems and verifies the validity of the proposed method.

2. Circuit Configuration

2.1 Piezoelectric Elements Figure 1 shows the size and structure of the piezoelectric element used in this paper: K7520BS3 from THRIVE. The right-hand side of the piezoelectric element is clamped and vibrated by a vibration source. On the other side of the piezoelectric element, the mass is tipped for the mechanical resonance to increase the amplitude.

The target application is the vibration of engines such as in a motor vehicle [29]. Thus, the vibration frequency is around 7000 rpm. In this paper, the frequency is assumed constant and set to 120 Hz. The problem of frequency change is left for future work.

Piezoelectric elements convert vibration energy into electric energy. The piezoelectric elements are expressed as shown in Fig. 2 (see [30]). The vibration energy and the piezoelectric ceramic are expressed in the AC current source and internal impedance as a capacitor and a resistor [30].

Table 1 lists the parameters of the vibration generators based on the 10 piezoelectric elements. Those parameters are measured from the result of a preliminary experiment.

2.2 All-passive Rectifier and *LC* Resonance

Fujiwara et al. [31] proposed a novel passive rectifier as shown in Fig. 3(a). Figure 3(a) is called as a boost-type current-improving passive rectifier. Figure 3(b) is a conventional diode bridge rectifier. We numerically compared and verified those all-passive rectifiers [32]. As the results, the boost-type current-improving passive rectifier is matched for the vibration generators based on the piezoelectric elements [32]. This paper proposes using a series inductor for *LC*

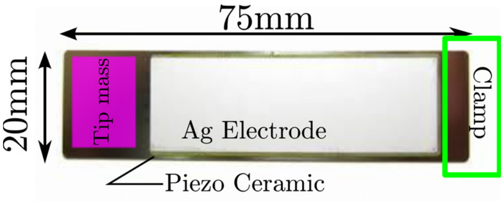

Fig. 1. Size and structure of the piezoelectric element used in this paper

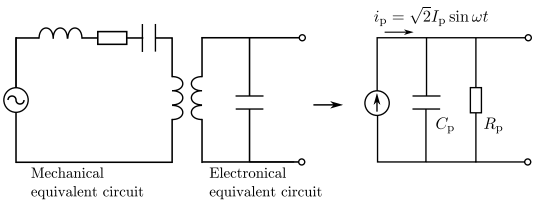

Fig. 2. Equivalent circuit of piezoelectric elements [30]

Table 1. Parameters of the 10 piezoelectric elements

I_p depends on vibration.	$\omega = 2\pi \times 120$ rad/s
$C_p = 1.06\,\mu$F	$R_p = 2.8\,\text{k}\Omega$

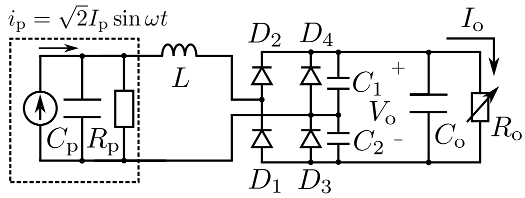

(a) Proposed circuit

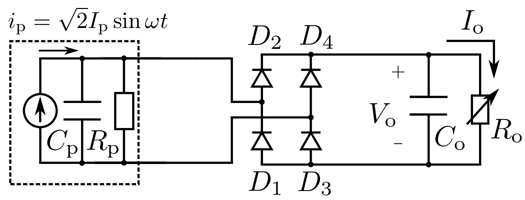

(b) Conventional circuit

Fig. 3. Proposed circuit and conventional circuit for vibration generators based on piezoelectric elements

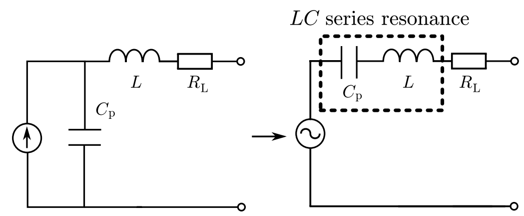

Fig. 4. Equivalent circuit of piezoelectric elements and a series inductor for *LC* resonance. R_L denotes a series resistor of inductor

resonance with the internal capacitor C_p from the piezoelectric elements to improve the output power.

Figure 4 describes the equivalent circuit of piezoelectric elements and a series inductor for *LC* resonance. Here, in the equivalent circuit of the piezoelectric elements, the internal resistor R_p is ignored because $1/R_p$ is too small.

The *LC* resonance equivalently reduces the internal capacitor C_p. At that time, the generator closes in the ideal power supply. As a result, the output power increases. This principle leads the optimal parameter of the inductor L. The follow equation holds: $\omega = 1/\sqrt{LC_p}$. In addition, we consider the effect of the internal resistor R_p:

$$\omega = \sqrt{\frac{1}{LC_p} - \left(\frac{1}{R_p C_p}\right)^2} \quad \cdots\cdots (1)$$

$$L = \frac{1}{\omega^2 C_p + 1/(R_p^2 C_p)} \approx 1.38\,\mathrm{H} \quad \cdots\cdots (2)$$

If the number of the piezoelectric elements is N times, C_p is N times and R_p is $1/N$ times. As a result, L becomes $1/N$ times from (2). As an example, when the number of the piezoelectric elements is set to 100 or 1000, L becomes 138 mH or 13.8 mH. In the future, if the number of the piezoelectric elements can increase for applications, the value and size of the inductor can be reduced.

This equation focuses on the only input side of Fig. 3(a). For the design of the parameters in the all-passive rectifier, it is necessary to consider the all systems in Fig. 3(a). The next section numerically addresses the design of parameters in Fig. 3(a). In addition, this proposed method has a big issue regarding the size of the inductor. Here, we have two ideas for the issue. One is a multi-mode vibration. The multi-mode vibrations [29] will provide the harmonics of the fundamental frequency. In other words, the vibration frequency ω becomes higher. The other is a large number of the piezoelectric elements. When these piezoelectric elements are parallelly connected for this system, the internal capacitance C_p becomes larger. To apply the two ideas is a future works for reducing the size of the inductor.

3. Design of Parameters

The maximum output power depends on the system parameters. In addition, the load would be changed by the applications. This section numerically addresses the design of parameters in Fig. 3(a). A circuit simulator called PLECS (ver. 3.7.5) was used for the numerical analysis.

At first, the respective parameters are explained. The RMS value of the AC current source I_p depends on the vibration. Here, I_p is assumed as 9.2 mA from the previous experiment [33]. The smoothing capacitor $C_o = 22\,\mu$F is enough larger than C_1 and C_2. We assume that the series and parallel resistors of the inductor, the capacitors, and the diodes are ignored. Furthermore, the forward voltage of the diodes is set to 0 V. Here, the parameters: L and $C = C_1 = C_2$ are changed in order to choose the optimal values.

Next, Fig. 5 describes the numerical results each load: R_o =1 kΩ, 2 kΩ, 3 kΩ, 4 kΩ, 5 kΩ, 7 kΩ, 9 kΩ, and 10 kΩ. The horizontal axis is the capacitance $C = C_1 = C_2$ every 0.01 μF and the vertical axis is the inductance L every 0.1 H in Fig. 5. The z-axis and its color in Fig. 5 draw the output power [mW]. Around $1.0\,\mathrm{H} < L < 2.5\,\mathrm{H}$ and $1.0\,\mu\mathrm{F} < C < 4.0\,\mu\mathrm{F}$, the output power becomes maximum. The reason why the inductance L has a narrow range for the large output power is the *LC* resonance from (2). (2) represents the matching parameter L for the *LC* resonance. However, the best point of the maximum output power would change every load condition. Then, this paper chooses the good parameters combination for widely load range from Fig. 5. Therefore, the inductance L and the capacitance C are set at around $1.75(=(1.0+2.5)/2)$ H and $2.5(=(1.0+4.0)/2)\,\mu$F The problem of the huge volume in this system remains for the future work.

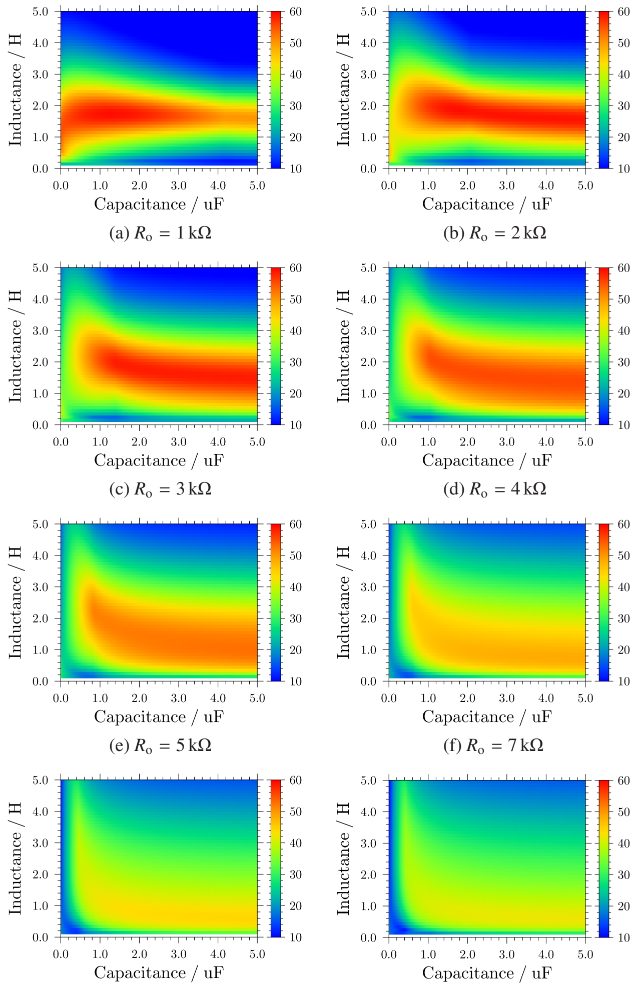

Fig. 5. Numerical results of output power [mW] in vibration generators each load: R_o =1 kΩ, 2 kΩ, 3 kΩ, 4 kΩ, 5 kΩ, 7 kΩ, 9 kΩ, and 10 kΩ. The color draws the output power [mW]

4. Verifications of Proposed Circuit

This section numerically and experimentally verifies the validity of the proposed circuit. In addition, the operations of the proposed circuit are described.

4.1 Setting of Conditions and Parameters Table 2 lists the parameters of the all-passive rectifier in Fig. 3(a). The series inductor L includes the series resistor R_L. The parameters of the inductor L and R_L (see Fig. 6) are measured by an impedance analyzer IM3570 (Hikoki, input voltage 5 Vrms): L = 1.70 H, R_L = 122.0 Ω. The capacitors of the all-passive rectifier C_1 and C_2 are set to 2.2 μF from Fig. 5. The smoothing capacitor C_o is 22 μF as well as previous section for both rectifiers in Fig. 3. The diodes of both rectifiers are ideal in the simulation and Schottky barrier diodes 1SS108 in the experimental system. A circuit simulator called PLECS (ver. 3.7.5) was used for the numerical analysis.

The vibration source and system configuration are explained. Figure 7 shows a photograph of the system. The 10 piezoelectric elements for vibration generators connect electrically in parallel and mechanically in a circular pattern. A

Table 2. Parameters of the all-passive rectifier

L = 1.70 H	R_L = 122.0 Ω	C_o = 22 μF
C_1 = 2.2 μF	C_2 = 2.2 μF	R_o variability

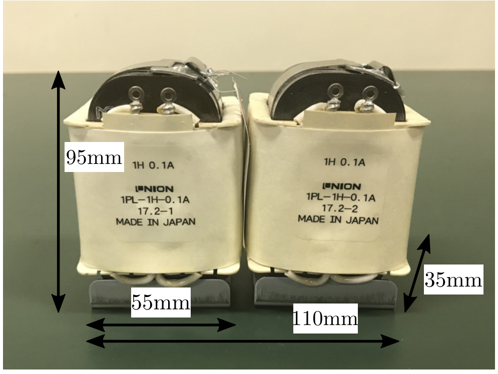

Fig. 6. Photograph of Inductor

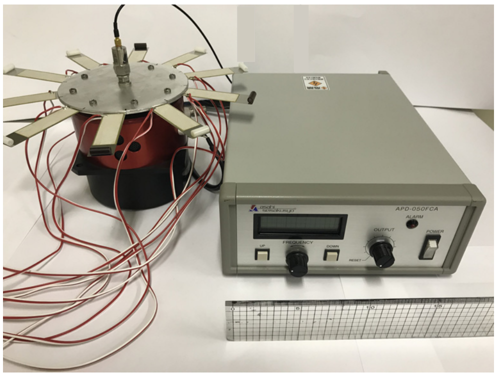

(a) Photograph

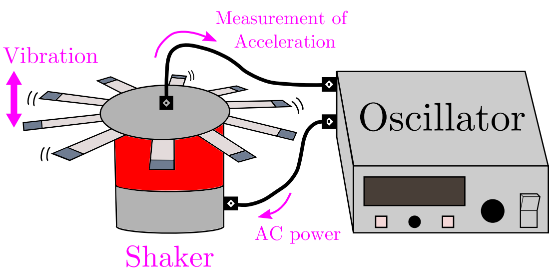

(b) Diagram

Fig. 7. Photograph and diagram of vibration generator with piezoelectric elements

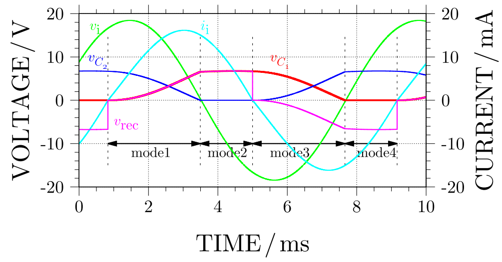

(a) R_o = 1 kΩ, V_o = 6.6 V

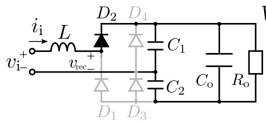

(b) mode 1

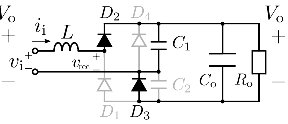

(c) mode 2

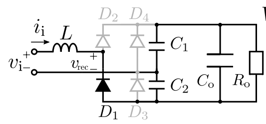

(d) mode 3

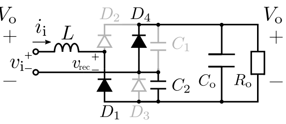

(e) mode 4

Fig. 8. Time waveforms and the operation modes in low-voltage region

shaker (SL-0505 in Fig. 7) vibrates the disk with the 10 piezoelectric elements. The shaker is driven by an AC power oscillator (APD-050FCA in Fig. 7).

4.2 Operation Analysis by Numerical Simulation

The all-passive rectifier has some operation modes every load. In this subsection, those operation modes are clarified by using numerical analysis. Here, I_p is assumed as 9.2 mA in the same setting as the section III. The numerical results show those operation modes and confirm *LC* resonance by phase shift between the current and the voltage. In the case of *LC* resonance, that is the impedance matching, the input current i_i and the input voltage v_i of the all-passive rectifier are shifted in phase by 90 degree. In addition, the power factor after the inductor L would become high. To confirm it, the voltage between the inductor and the diode bridge is defined as v_{rec}. The voltage v_{rec} and the input current i_i are compared about those phases.

In the low-voltage region, Fig. 8(a) represents the time waveforms and Figs. 8(b)–(e) illustrate the operation modes of Fig. 8(a). In mode 1, only the diode D_2 conducts. Therefore, the voltages v_{rec} and v_{C_1} are same shapes. The charging current flows to the capacitor C_1 and the discharging current flows through the load R_o to the capacitor C_2. When the capacitors C_1 and C_2 finish charging and discharging, mode 1 shifts to mode 2. In mode 2, the diodes D_2 and D_3 conduct: the diode D_3 turns on from mode 1. As the capacitor C_1 connects the smoothing capacitor C_o in parallel, the voltage v_{C_1} keeps constant during the positive input current $i_i > 0$. When the input current i_i becomes zero, mode 2 shifts to mode 3. At that time, v_i keeps sinusoidal though v_{rec} is like a ladder shape. The reason is the shape of the current i_i. The equation $v_i = L\mathrm{d}i_i/\mathrm{d}t + v_{rec}$ holds. By enlarging the waveform of i_i, it is bent at mode change. Therefore, $L\mathrm{d}i_i/\mathrm{d}t$ sharply changes as well as v_{rec}. This phenomenon would happen in the later results. In mode 3, the diodes D_2 and D_3 do not conduct and the diode D_1 turns on. Therefore, the voltages v_{rec} and $-v_{C_2}$ are same shapes. Mode 3 is an inverted mode 1. In mode 4, the diodes D_1 and D_4 conduct: the diode D_4 turns on from mode 3. Mode 4 is an inverted mode 2 in same way of mode 3.

The higher load R_o becomes from the low-voltage region, the shorter mode 2 and mode 4 of Fig. 8 get. In the middle-voltage region, mode 2 and mode 4 of Fig. 8 disappear. Figure 9(a) represents the time waveforms and Figs. 9(b)–(c) illustrate the operation modes of Fig. 9(a). In mode 1, only the diode D_2 conducts. Therefore, the voltages v_{rec} and v_{C_1} are same shapes. Mode 1 of Fig. 9(b) and mode 1 of Fig. 8(b) are same operation modes. When the input current i_i becomes zero before the capacitors C_1 and C_2 finish charging and discharging, mode 1 shifts to mode 2. Therefore, the voltages v_{C_1} and v_{C_2} do not reach zero. In mode 2, the diode D_2 turn off and the diode D_1 turns on from mode 1. Mode 2 of Fig. 9(c) and mode 3 of Fig. 8(d) are same operation modes. Mode 2

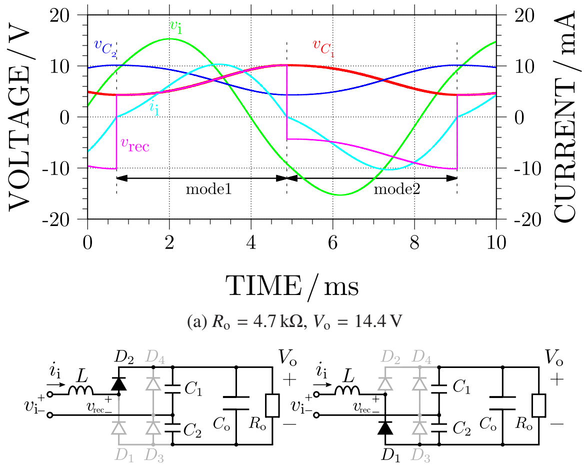

(a) R_o = 4.7 kΩ, V_o = 14.4 V

(b) mode 1　　(c) mode 2

Fig. 9. Time waveforms and the operation modes in middle-voltage region

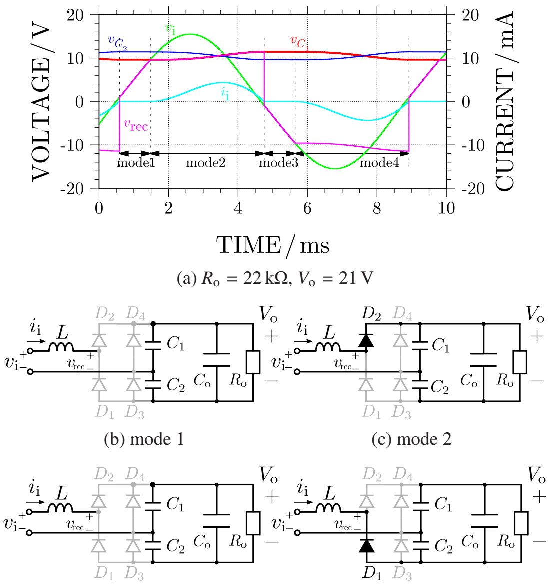

(a) R_o = 22 kΩ, V_o = 21 V

(b) mode 1　　(c) mode 2

(d) mode 3　　(e) mode 4

Fig. 10. Time waveforms and the operation modes in high-voltage region

is an inverted mode 1.

In the high-voltage region, Fig. 10(a) represents the time waveforms and Figs. 10(b)–(e) illustrate the operation modes of Fig. 10(a). All diodes D_1, D_2, D_3, and D_4 do not conduct. Therefore, the voltages v_{rec} and v_i are same shapes. As the capacitors C_1 and C_2 connect the smoothing capacitor C_o in parallel, the voltages v_{C_1} and v_{C_2} keep constant during $v_i < v_{C_1}$. When the input voltage v_i reaches the capacitor voltage v_{C_1}, the diode D_2 turns on and mode 1 shifts to mode 2. In mode 2, only the diode D_2 conducts. Therefore, the voltages v_{rec} and v_{C_1} are same shapes and the input current i_i starts to flow. The charging current flows to the capacitor C_1 and the discharging current flows through the load R_o to the capacitor C_2. After the input voltage v_i becomes lower than the capacitor voltage v_{C_1}, the input current i_i starts to decrease. When the input current i_i becomes zero, the diode D_2 turns off and mode 2 shifts to mode 3. In mode 3, all diodes D_1, D_2, D_3, and D_4 do not conduct. Therefore, the voltages v_{rec} and v_i are same shapes. Mode 3 is an inverted mode 1. When the input voltage v_i reaches the inverted capacitor voltage $-v_{C_2}$, the diode D_1 turns on and mode 3 shifts to mode 4. In mode 4, only the diode D_1 conducts. Therefore, the voltages v_{rec} and $-v_{C_2}$ are same shapes and the input current i_i starts to flow. Mode 4 is an inverted mode 2 in same way of mode 3.

The loss and the efficiency are discussed in Figs. 8, 9 and 10. Table 3 lists these parameters by numerical simulation. In this case, the inductor loss is dominant because the other compartments: capacitors and diodes are ideal devices.

Table 3. Inductor loss and efficiency in Figs. 8, 9 and 10 by numerical simulation

Load resistor	Input power	Output power	Inductor loss	Efficiency
1 kΩ	59.10 [mW]	43.56 [mW]	15.54 [mW]	73.7%
4.7 kΩ	50.28 [mW]	44.32 [mW]	5.96 [mW]	88.1%
22 kΩ	20.84 [mW]	20.06 [mW]	0.78 [mW]	96.3%

Finally, this section focuses on the phase shift between the current and the voltage waveforms. In Figs. 8 and 9, the input current i_i and the input voltage v_i are shifted in phase by less than 90 degree. It means the *LC* series resonance between the internal capacitor C_p and the series inductor L. In addition, in all results of Figs. 8, 9, and 10, the signs of the input current i_i and the voltage v_{rec} are equal. Therefore, the all-passive rectifier after the series inductor L keeps high power factor. This effect improves the output characteristics for the vibration generators based on the piezoelectric elements.

4.3 Operation Waveforms of Prototype System

This subsection verifies the proposed circuit operation in the prototype system. Figure 11 depicts the voltage waveforms† in the prototype system when the load resistor R_o = 1 kΩ, 4.7 kΩ, 22 kΩ. Figure 11 has the mode added in the figure to match Figs. 8, 9 and 10. The results show that the pulsation of the capacitor voltage determines whether the diode is ON/OFF and the circuit is operating.

4.4 *I-V* and *P-V* Output Characteristics of Prototype System

This subsection shows *I-V* and *P-V* output characteristics of Fig. 3 for effect of the proposed method. Figure 12 represents the numerical and experimental results: the lines are the numerical results and the points are the experimental results. Figures 12(a) and (b) describe *I-V* and *P-V* output characteristics. The shapes of those graphs are similar between the conventional and proposed results. However, the maximum value of the output voltage and power in the proposed circuit become higher and larger than the conventional one. The reason is that the previous subsection showed the *LC* series resonance for improvement in the output characteristics.

The characteristics of the proposed circuit are considered for each voltage region. In the low-voltage region, the operation modes are Fig. 8. The operation has the modes of both the diode bridge and the voltage doubler rectifiers. In addition, the operation has no term of non-conduction. Therefore, the proposed circuit provides larger current than the conventional one. In the middle-voltage region, the operation modes are Fig. 9. Although the operation is the same as the voltage doubler rectifier, the operation has no term of non-conduction

† The input current cannot be measured by an AC current sensor because it is too small to be measured. In the next subsection, the output current is measured by the shunt resistor, included in the load resistor.

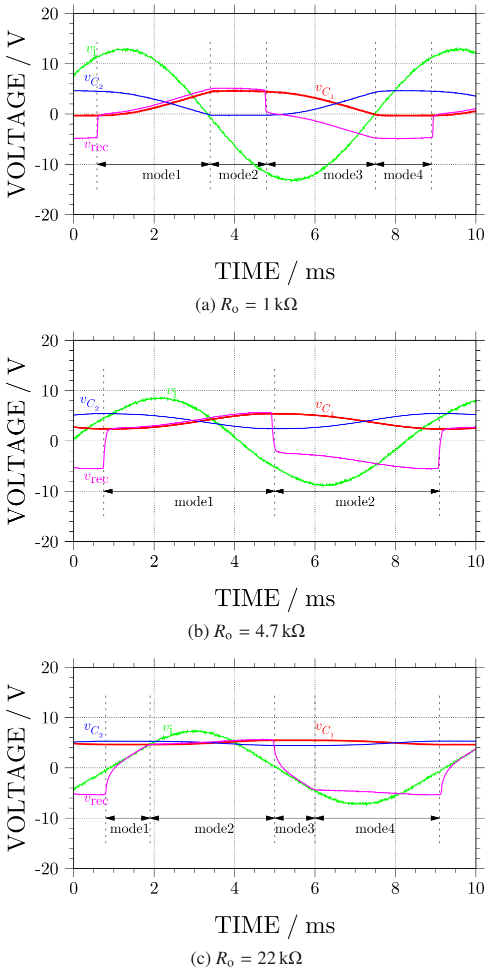

(a) R_o = 1 kΩ

(b) R_o = 4.7 kΩ

(c) R_o = 22 kΩ

Fig. 11. Voltage waveforms in prototype system

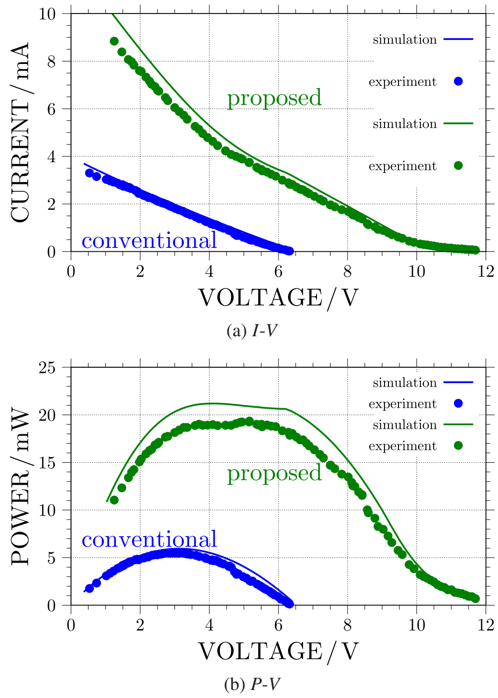

(a) *I-V*

(b) *P-V*

Fig. 12. Numerical and experimental results of *I-V* and *P-V* output characteristics in conventional and proposed circuits of Fig. 3

by the series inductor *L*. In the high-voltage region, the operation modes are Fig. 10. The operation is the typical voltage doubler rectifier modes. In the middle/high-voltage region, the proposed results of Fig. 12 have difference between the numerical and the experimental results. An impedance analyzer: IM3570 (Hioki, input voltage 5 Vrms) measured the parameters *L* and R_L for numerical analysis. However, it is well known that the parameters of the inductor may change depending on the voltage, Therefore, the numerical and the experimental results have the little difference, but the difference does not affect the proposed methods for improvement of the vibration generators based on the piezoelectric elements.

5. Summary

This paper has investigated the improvement in the output voltage and power from the vibration generator based on piezoelectric elements by using all-passive rectifier. The input series inductor resonated the internal capacitor of the piezoelectric elements and equivalently reduced it. As the results, the output power of the proposed circuit increased compared with the conventional circuit. In addition, those operations were numerically analyzed in detail.

In this paper, the novelty is to use electronic resonance in the vibration generators consisted of the piezoelectric elements without the additional resonator circuit. In addition, the results in this paper contribute the numerical and experimental verifications of the proposed method.

The problems of system volume and frequency shift remain for the future work.

Acknowledgment

The authors would like to thank to Mr. Akito Nakagaki and Mr. Genki Hase for their supports about the additional numerical simulations and experimentation in this paper.

References

(1) P. Spies, M. Pollak, and L. Mateu: *Handbook of Enetgy Harvesting Power Supplies and Applications*, 1st ed. Pan Stanford, ch. 1 (2015)

(2) N. Zhao, S. Zhang, F.R. Yu, Y. Chen, A. Nallanathan, and V. CM Leung: "Exploiting interference for energy harvesting: A survey, research issues, and challenges", *IEEE Access*, Vol.5, pp.10403–10421 (2017)

(3) S. Priya, H.-C. Song, Y. Zhou, R. Varghese, A. Chopra, S.-G. Kim, I. Kanno, L. Wu, D.S. Ha, J. Ryu, and R.G. Polcawich: "A review on piezoelectric energy harvesting: materials, methods, and circuits", *Energy Harvesting and Systems*, Vol.4, No.1, pp.3–39 (2017)

(4) R. Ahmed, F. Mir, and S. Banerjee: "A review on energy harvesting approaches for renewable energies from ambient vibrations and acoustic waves using piezoelectricity", *Smart Materials and Structures*, Vol.26, No.8, pp.085 031–085 058 (2017)

(5) S.R. Platt, S. Farritor, and H. Haider: "On low-frequency electric power generation with PZT ceramics", *IEEE/ASME Transactions on Mechatronics*, Vol.10, No.2, pp.240–252 (2005)

(6) J.M. Donelan, Q. Li, V. Naing, J. Hoffer, D. Weber, and A.D. Kuo: "Biomechanical energy harvesting: generating electricity during walking with minimal user effort", *Science*, Vol.319, No.5864, pp.807–810 (2008)

(7) L. Mateu and F. Moll: "Appropriate charge control of the storage capacitor in a piezoelectric energy harvesting device for discontinuous load operation", *Sensors and Actuators A: Physical*, Vol.132, No.1, pp.302–310 (2006)

(8) J. Granstrom, J. Feenstra, H.A. Sodano, and K. Farinholt: "Energy harvesting from a backpack instrumented with piezoelectric shoulder straps", *Smart Materials and Structures*, Vol.16, No.5, pp.1810–1820 (2007)

(9) S. Priya: "Modeling of electric energy harvesting using piezoelectric windmill", *Applied Physics Letters*, Vol.87, No.18, p.184101 (2005)

(10) S. Pobering and N. Schwesinger: "A novel hydropower harvesting device", in *International Conference on MEMS, NANO, and Smart Systems*, IEEE,

pp.480–485 (2004)
(11) S. Oh, H. Han, S. Han, J. Lee, and W. Chun: "Development of a tree-shaped wind power system using piezoelectric materials", *International Journal of Energy Research*, Vol.34, No.5, pp.431–437 (2010)
(12) H.S. Kim, J. Kim, and J. Kim: "A review of piezoelectric energy harvesting based on vibration", *International Journal of Precision Engineering and Manufacturing*, Vol.12, No.6, pp.1129–1141 (2011)
(13) G.K. Ottman, H.F. Hofmann, A.C. Bhatt, and G.A. Lesieutre: "Adaptive piezoelectric energy harvesting circuit for wireless remote power supply", *IEEE Transactions on Power Electronics*, Vol.17, No.5, pp.669–676 (2002)
(14) G.K. Ottman, H.F. Hofmann, and G.A. Lesieutre: "Optimized piezoelectric energy harvesting circuit using step-down converter in discontinuous conduction mode", *IEEE Transactions on Power Electronics*, Vol.18, No.2, pp.696–703 (2003)
(15) N. Kong, D.S. Ha, A. Erturk, and D.J. Inman: "Resistive impedance matching circuit for piezoelectric energy harvesting", *Journal of Intelligent Material Systems and Structures*, Vol.21, No.13, pp.1293–1302 (2010)
(16) A. Romani, M. Filippi, and M. Tartagni: "Micropower design of a fully autonomous energy harvesting circuit for arrays of piezoelectric transducers", *IEEE Transactions on Power Electronics*, Vol.29, No.2, pp.729–739 (2014)
(17) D. Guyomar, A. Badel, E. Lefeuvre, and C. Richard: "Toward energy harvesting using active materials and conversion improvement by nonlinear processing", *IEEE Transactions on Ultrasonics, Ferroelectrics, and Frequency Control*, Vol.52, No.4, pp.584–595 (2005)
(18) Y.K. Ramadass and A.P. Chandrakasan: "An efficient piezoelectric energy harvesting interface circuit using a bias-flip rectifier and shared inductor", *IEEE Journal of Solid-State Circuits*, Vol.45, No.1, pp.189–204 (2010)
(19) L. Wu, X.-D. Do, S.-G. Lee, and D.S. Ha: "A self-powered and optimal SSHI circuit integrated with an active rectifier for piezoelectric energy harvesting", *IEEE Transactions on Circuits and Systems I: Regular Papers*, Vol.64, No.3, pp.537–549 (2017)
(20) I. Lien, Y. Shu, W. Wu, S. Shiu, and H. Lin: "Revisit of series-sshi with comparisons to other interfacing circuits in piezoelectric energy harvesting", *Smart Materials and Structures*, Vol.19, No.12, p.125009 (2010)
(21) S. Lu and F. Boussaid: "A highly efficient p-sshi rectifier for piezoelectric energy harvesting", *IEEE Transactions on Power Electronics*, Vol.30, No.10, pp.5364–5369 (2015)
(22) G.A. Rincón-Mora and S. Yang: "Tiny piezoelectric harvesters: Principles, constraints, and power conversion", *IEEE Transactions on Circuits and Systems I: Regular Papers*, Vol.63, No.5, pp.639–649 (2016)
(23) D. Kwon and G.A. Rincon-Mora: "A rectifier-free piezoelectric energy harvester circuit", in *IEEE International Symposium on Circuits and Systems, 2009. ISCAS 2009.* IEEE, pp.1085–1088 (2009)
(24) C. Peters, J. Handwerker, D. Maurath, and Y. Manoli: "A sub-500 mv highly efficient active rectifier for energy harvesting applications", *IEEE Transactions on Circuits and Systems I: Regular Papers*, Vol.58, No.7, pp.1542–1550 (2011)
(25) M. Minami, A. Nakagaki, and G. Hase: "A Numerical Analysis of Current Waveforms in Circulating Current Control Circuit with the Third Harmonics for Vibration Generator", in *Proceedings of 2019 IEEE 8th Global Conference on Consumer Electronics (GCCE 2019)*, pp.555–557 (2019)
(26) M. Minami, A. Nakagaki, and G. Hase: "An Experimental Analysis of Circulating Current Control Circuit for Output Power from Vibration Generator for Vibration including the Third Harmonics", in *Proceedings of the 22th European Conference on Power Electronics and Applications (EPE'20 ECCE Europe)* (2020)
(27) L. Costanzo, A. Lo Schiavo, and M. Vitelli: "Power maximization from resonant electromagnetic vibration harvesters feeding bridge rectifiers", *International Journal of Circuit Theory and Applications* (2018)
(28) M. Minami: "Improvement in output characteristics using a resonator and passive rectifiers in vibration generators", *IEEE Transactions on Power Electronics*, Vol.34, No.8, pp.7184–7191 (2019)
(29) S. Hashimoto, N. Nagai, Y. Fusikura, J. Takahashi, S. Kumagai, M. Kasai, K. Suto, and H. Okada: "Multi-mode vibration-based power generation for autombiles", in *Proceedings of the Industry Applications Society Annual Meeting* (2012)
(30) S. Roundy and P.K. Wright: "A piezoelectric vibration based generator for wireless electrinics", *Institute of Physics Publishing Smart Materials Structures*, Vol.13, pp.1131–1142 (2004)
(31) K. Fujiwara and H. Nomura: "A new operating principle of voltage-doubler diode rectifiers to meet the harmonic guide lines (in Japanese)", *IEEJ Transactions on Industry Applications*, Vol.119, No.1, pp.103–108 (2008)
(32) T. Sakabe, M. Minami, S. Motegi, and M. Michihira: "A numerical analysis and improvement of output characteristics in different passive rectifiers based on vibration generators", in *Proceedings of The 2018 International Power Electronics Conference -ECCE Asia-* (2018)
(33) M. Minami, T. Sakabe, S. Motegi, and M. Michihira: "An experimental verification for improvement of output characteristics by LC resonance in vibration generators with boost-type current-improving passive rectifier", in *Proceedings of 7th International Conference on Renewable Energy Research and Application (ICRERA 2018)* (2018)

Masataka Minami (Member) received the Bachelor's, Master's, and Ph.D. degrees from Kyoto University, Kyoto, Japan, in 2008, 2010, and 2013, respectively. In 2013, he joined the Department of Electrical Engineering, Kobe City College of Technology (KCCT), where he is currently an Associate Professor. From April 2018 to March 2019, he was an Academic Visitor in the School of Engineering, Ecole Polytechnique Federale de Lausanne (EPFL), Lausanne, Switzerland. His research interests include rectifiers, DC/DC converters, inverters, power systems engineering, and control applications. He received the IEEJ Industry Applications Society Excellent Presentation Award in 2017 and the IEEE GCCE 2019 Excellent Poster Award; Outstanding Prize in 2019. He is a member of the Institute of Electronics, Information and Communication Engineers (IEICE) and Institute of System, Control and Information Engineers (ISCIE).

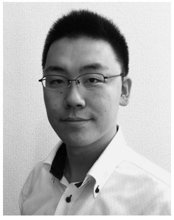

Koharu Kondo (Student Member) received the Associate's degree from the Department of Electrical Engineering, Kobe City College of Technology (KCCT) in 2019. Since 2019, she is a Bachelor of the Department of Electrical, Electronics and Information Engineering, Nagaoka University of Technology, Japan.

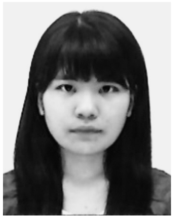

Shin-ichi Motegi (Member) received the Master's and Ph.D. degrees from Tokyo Denki University, Saitama, Japan, in 1996 and 2002, respectively. From 2003 to 2012, he was with YANMAR Co., Ltd., Shiga, Japan. In 2012, he joined Tokyo Denki University as a research associate in the Department of Electrical and Electronic Engineering. Since 2013, he joined the Department of Electrical Engineering, Kobe City College of Technology (KCCT), where he is currently a Professor. His research interests are rectifier, DC/DC converter, inverter, and control applications. He is a member of the Institute of Electrical and Electronics Engineers (IEEE), the Institute of Electronics, Information and Communication Engineers (IEICE), the Japan Institute of Power Electronics (JIPE), and the Institute of Electrical Installation Engineers of Japan (IEIEJ).

Masakazu Michihira (Member) received Master's degree from Kobe University, Hyogo, Japan in 1995 and Ph.D. degree from Osaka University, Osaka, Japan in 1998. Since 1998, he joined the Department of Electrical Engineering, Kobe City College of Technology (KCCT), where he is currently a Professor. His research interests are DC/DC converter, DC/AC converter, and control applications. He is a member of the Institute of Electrical and Electronics Engineers (IEEE) and the Japan Institute of Power Electronics (JIPE).